Nonlinear Raman–Nath diffraction of femtosecond laser pulses

A. M. Vyunishev,[1,2,*] V. V. Slabko,[2] I. S. Baturin,[3,4] A. R. Akhmatkhanov,[3,4] and V. Ya. Shur[3,4]

[1]*L.V. Kirensky Institute of Physics, 660036 Krasnoyarsk, Russia*

[2]*Siberian Federal University, 660079 Krasnoyarsk, Russia*

[3]*Ural Federal University, 620000 Ekaterinburg, Russia*

[4]*Labfer Ltd., 620014 Ekaterinburg, Russia*

**Corresponding author: vyunishev@iph.krasn.ru*

Received May 29, 2014; revised June 13, 2014; accepted June 13, 2014;
posted June 17, 2014 (Doc. ID 211960); published July 14, 2014

We study the nonlinear Raman–Nath diffraction (NRND) of femtosecond laser pulses in a 1D periodic nonlinear photonic structure. The calculated second-harmonic spectra represent frequency combs for different orders of transverse phase matching. These frequency combs are in close analogy with the well-known spectral Maker fringes observed in single crystals. The spectral intensity of the second harmonic experiences a redshift with a propagation angle, which is opposite the case of Čerenkov nonlinear diffraction. We analyze how NRND is affected by the group-velocity mismatch between fundamental and second-harmonic pulses and by the parameters of the structure. Our experimental results prove the theoretical predictions.

OCIS codes: (190.2620) Harmonic generation and mixing; (190.4223) Nonlinear wave mixing; (160.4330) Nonlinear optical materials.

http://dx.doi.org/10.1364/OL.39.004231

When a monochromatic wave propagates through a refractive index grating, either Bragg or Raman–Nath diffraction takes place. A similar situation occurs when a homogenous optical medium possesses periodical modulation of second-order nonlinear susceptibility forming a nonlinear grating. In this case, nonlinear Bragg diffraction and nonlinear Raman–Nath diffraction (NRND) can be observed [1–4]. Nonlinear Bragg diffraction appears when phase mismatch $\Delta\mathbf{k}$ between the double fundamental wave vector $2\mathbf{k}_1$ and second-harmonic wave vector $\mathbf{k}_2$ is strictly compensated by the reciprocal lattice vector $\mathbf{G}$ (RLV) of the structure $\Delta\mathbf{k} = 2\mathbf{k}_1 - \mathbf{k}_2 = m\mathbf{G}$, where m is an integer being the order of transverse quasi-phase-matching. Although in most practical cases this condition fails, one can observe less efficient second-harmonic generation (SHG), which is due to Čerenkov nonlinear diffraction (CND) [5–15] when only longitudinal components are involved $k_2 \cos\theta = 2k_1$, where θ is the inner emission angle of the second harmonic (SH) with respect to the fundamental propagation direction. On the contrary, NRND occurs when only transverse components of wave vectors are matched by RLV, such that $k_2 \sin\beta_m = mG_0$. In this case, multiple second-harmonic beams diffract on the nonlinear grating at the angles β_m [3]. Being incompletely phase matched, any one of these types of phase matching attracts much attention in view of wide tunability in the spectral and angular ranges. It should be emphasized that SHG, due to nonlinear Bragg diffraction, is possible in the case when the CND angle is equal to one of the NRND angles ($\theta = \beta_m$), which imposes restrictions on the parameters of the nonlinear grating, the operating wavelengths, and the incidence angles of the fundamental beam. An elegant analysis of interrelation between these processes can be found in [4]. The study of CND as well as nonlinear Bragg diffraction has been the subject of numerous prominent works [1–15], whereas NRND still remains an understudied phenomenon. The first observation of SHG via NRND was reported in [2]. A series of experiments, where quasi-monochromatic waves were used as a fundamental source, were performed by the authors of [2–4]. Although ultrashort laser pulses were used in recent works [16,17], a detailed treatment of their conversion via NRND is still lacking. We believe that such treatment will enrich our knowledge of this phenomenon and prove the recent theoretical analysis to be correct [18].

In this Letter, we report our study of SHG of femtosecond laser pulses under NRND. The sample under study was a 1D periodic nonlinear photonic structure based on an uniaxial ferroelectric congruent lithium niobate (CLN) crystal with the dimensions 11 mm × 2 mm × 0.5 mm fabricated by an electric-field poling procedure using a lithographically defined photoresist grating [19] (Labfer Ltd.). Its second-order nonlinear susceptibility was modulated along the x axis with a period of $\Lambda = 10$ μm, as shown in Figs. 1(a) and 1(b). Fundamental radiation from a Ti:sapphire oscillator (Tsunami, Spectra-Physics), delivering 100 fs pulses at a repetition rate of 80 MHz, is directed at a small angle to the y axis of CLN. The fundamental radiation was focused with a 20 cm lens into the sample to provide a 78 μm focal beam spot. Polarization of the fundamental radiation was chosen along the z axis to employ the highest nonlinear coefficient d_{33}. This configuration is not common, as follows from the previous works, but in our case we have no restrictions on the sample size imposed by the poling technique (thickness is limited to 0.5 mm for CLN crystals due to a high coercive field). It is expected that increasing the nonlinear interaction length will strengthen the effects associated with the ultrashort pulse interaction and improve the spectral characteristics of SH.

A complete analysis of SHG of femtosecond pulses via NRND can be done in terms of the recent theoretical model [7]. It has been proved experimentally that this

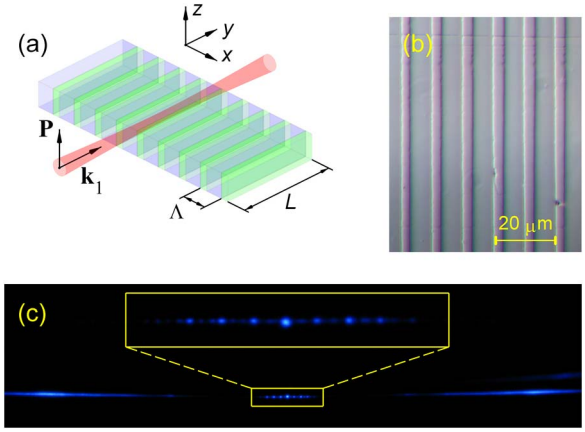

Fig. 1. (a) Experimental scheme. (b) Part of etched polar surface of the sample. (c) SH pattern on the screen (inset: expanded view of NRND). Peripheral and central SH spots correspond to CND and NRND, respectively.

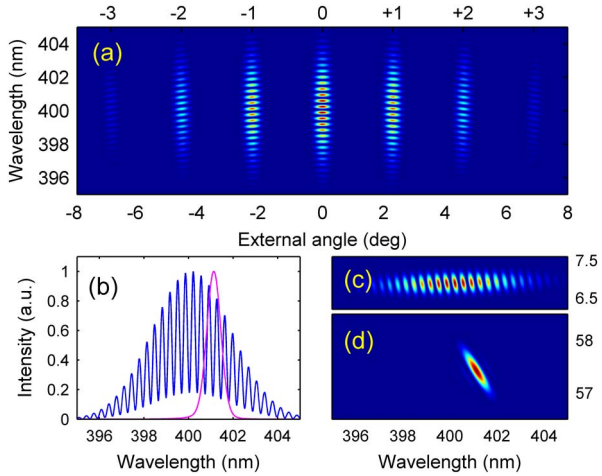

Fig. 2. (a) Calculated angular distribution of SH spectral intensity for the parameters: $w = 40$ μm, $L = 400$ μm, $D = 0.75$ (top scale corresponds to NRND order). (b) SH spectra averaged over the angle for NRND ($m = \pm 3$, blue) and CND ($m = \pm 21$, pink). (c) and (d) Local angular plots of SH spectral intensity for NRND of the third order ($m = \pm 3$) and CND ($m = \pm 21$), respectively. The vertical scale corresponds to the propagation angle.

model is adequate to calculate spectral and angular characteristics of SH radiation generated under a CND condition [7,13,14]. In the current study, we will address the cases of lower-order transverse phase matching in which a series of SH beams is emitted at relatively small angles with respect to the fundamental beam [Fig. 1(c)]. The SH spectral intensity generated at the distance y inside the structure under slowly varying amplitude approximation and in the low conversion limit can be represented in the form [7]:

$$S(\Omega, K, y) = (|\alpha y|)^2 \exp\left(-\frac{\tau^2\Omega^2}{4}\right) \times \operatorname{sinc}\left(\frac{y}{2}\left[\Delta k + \nu\Omega - \frac{K^2}{2k_2}\right]\right)^2 R(K), \quad (1)$$

where $\alpha = (\pi/2)^{3/2}\tau a^2\Gamma$, $\Gamma = -i\beta_2 I_1$, $\beta_2 = 2\pi k_2 \chi^{(2)}/n_2^2$, 2τ and a are the fundamental pulse duration and the focal spot radius at the $1/e$ field strength point, $\Omega = \omega_2 - 2\omega_{10}$ is the frequency detuning with ω_{10} being the central frequency of the fundamental wave, $\nu = (u_2^{-1} - u_1^{-1})$ is the group-velocity mismatch, and n_j denotes the refractive index of CLN at respective frequency $j\omega$ ($j = 1, 2$), which can be found in [20]. The product $\nu\Omega$ governs the temporal walk-off between fundamental and second-harmonic pulses owing to the group-velocity mismatch. The function

$$R(K) = \left(\sum\nolimits_m g_m \exp[-a^2(mG_0 + K)^2/8]\right)^2 \quad (2)$$

represents the Fourier transform of the nonlinear grating, where K is the spatial frequency, while $G_0 = 2\pi/\Lambda$ is the primary RLV. Fourier coefficients g_m for a periodic nonlinear grating with the duty cycle D take the form $g_m = 2D - 1$ if $m = 0$ and $g_m = 2\sin(\pi m D)/\pi m$ otherwise. The fundamental beam focal spot size is given by $w = (2\ln 2)^{1/2}a$. Note that for quasi-monochromatic waves, Eq. (1) essentially can be simplified [18].

It is convenient to use the solution of Eq. (1) in the coordinates of the SH propagation angle and the wavelength. In this case, the spatial frequency and internal SH propagation angle are interrelated through $K = 4\pi n_2 \sin(\theta)/\lambda$, where λ is the fundamental wavelength. Figure 2(a) shows angular dependence of the SH spectral intensity at the central fundamental wavelength 800 nm. As one can see, the SH spectral intensity plot contains multiple angular peaks (corresponding to different orders m), which can be attributed to NRND in a periodic structure. It is appropriate to introduce the definition of a local spectrum, which is a spectrum at a given propagation angle rather than the angle-averaged spectrum. The local SH spectrum is a set of peaks within the overall spectrum corresponding to the fundamental radiation (the so-called spectral fringes). In fact these spectral peaks represent the well-known spectral Maker fringes observed in a single crystal away from phase matching [21]. The mathematical reason behind these spectral peaks is oscillation of the sinc function in Eq. (1), which occurs each time the argument is changed by 2π. This leads to oscillation of the energy flow between fundamental and SH waves along the propagation distance. The period of such oscillations is equal to the double coherence length given by $l_{\mathrm{coh}} = \pi/(\Delta k + \nu\Omega - K^2/2k_2)$. The factor $\nu\Omega$ accounts for the contribution of the group-velocity mismatch between the fundamental and SH pulses. As a result, the width and spacing between the spectral peaks are smaller than those in the case of continuous waves when the factor $\nu\Omega$ is omitted. It is worth noting that the spectral width and spacing are also decreasing with the increasing of propagation distance. Angular averaging of the SH spectral intensity results in overlapping of adjacent peaks, causing ripples for low-order phase matching [Fig. 2(b), blue curve] and yielding a smooth spectrum for higher-order phase matching. Analysis of Eq. (1) suggests that better overlapping of adjacent peaks is assured when the sample is thick enough and the fundamental radiation is tightly

focused into the structure, providing a smooth averaged SH spectrum. This is mainly due to the wider angular bandwidth of SH achieved in this case. As depicted in Figs. 2(a) and 2(c), the spectral intensity of SH experiences quite a small redshift with the propagation angle. The origin of this spectral shift can be understood in terms of the condition for NRND: $\sin \beta_m = m\lambda/\Lambda$; thus the longer the wavelength, the larger the propagation angle. Note that the spectral shift grows with the order of transverse phase matching. However, the sign of this spectral shift is opposite to the one corresponding to CND, as shown in Figs. 2(c) and 2(d). In the case of CND, the transverse phase mismatch is not strictly compensated by RLV under numerical conditions, and the SH spectral intensity maximum shifts toward higher wavelengths [Fig. 2(b)]. This shift can be compensated by a proper choice of the structure period. The spectral width is mainly limited by the fundamental beam spot size as reported in [14].

Figure 3 illustrates measured angular dependence of the averaged SH power. This dependence is symmetric despite the slightly oblique incidence of the fundamental beam on the sample (less than 1 deg). It recently has been shown experimentally and theoretically [3,4] that changing the incidence angle does not affect the respective amplitudes of SH beams, at least within an angular range of 10 deg. The average SH powers corresponding to beams with $m = \pm 2$ are equal and therefore can be used in the fitting procedure for calculated and measured dependences. It has recently been shown [18] that the SH power corresponding to different orders depends not only on the duty cycle but also on the sample thickness. This requires precise measurements of the sample thickness. However, for broadband pumping, we can expect that the corresponding angular distribution of SH power will not depend on the thickness of a sample because of the many spectral components involved, and averaging over the spectrum gives us the same powers of specific SH beams for different thicknesses. Thus distribution of the average power among different SH peaks will be governed by the duty cycle value, which influences the respective Fourier coefficients. For these purposes, SH beams of order $m = 0, \pm 2$ were chosen to satisfy the condition $(P^0/P^{\pm 2})_{\text{calc}} = (P^0/P^{\pm 2})_{\text{exp}}$. The best agreement between the fitted and measured dependences was achieved at the duty cycle $D \approx 0.815$. The retrieved value of the duty cycle agrees well with the value ~0.8 obtained from the optical images of the etched polar surface of the sample, as shown in Fig. 1(b). The result of this fitting is shown in Fig. 3. Some disagreement is observed for the SH beams with $m = \pm 1$. This disagreement may appear due to the periodicity breaking of the structure in accordance with [17,18]. Note that the angular widths of the calculated and measured dependences are in good agreement with each other. The following data from the experiment were used for our calculations: 800 nm central fundamental wavelength, 78 μm fundamental beam spot size, 80 fs fundamental pulse duration, and $L = 2$ mm crystal length in the propagation direction. The inset in Fig. 3 illustrates the $m = +2$ SH beam profile. The intensity distribution across the SH beam cross section is adequately described by the Gaussian function. Using a laser beam profiler LBP-1 (Newport Corp.) mounted on a linear translation stage, we measured the angles of SH beam propagation corresponding to different orders of NRND. We clearly observed the first five orders. These results and the data calculated using the formula $\sin \beta_m = m\lambda/\Lambda$ are summarized in Table 1. The calculated data are in good correspondence with the measured ones. It also has been proved that the passed fundamental beam remains unchanged behind the sample, ensuring no change of the CLN refractive index, which could be induced by high intensity.

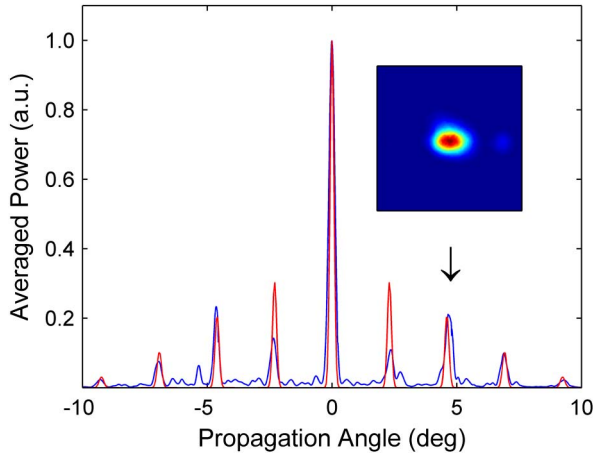

Fig. 3. Measured (blue) and calculated (red) angular dependences of SH intensity integrated over the spectrum. Inset: SH beam profile ($m = +2$).

Figure 4(a) shows the calculated and measured spectra, corresponding to SH beams with order $m = +2$. The calculated spectrum consists of a number of narrow-width peaks (green curve), which cannot be resolved by the spectrometer used. Despite this, averaging within the 0.5 nm spectral window leads to smoothing of the SH spectrum (black curve). As a result, the averaged calculated SH spectrum is in good agreement with the measured one (blue curve). Figures 4(b) and 4(c) show measured SH spectra for NRND orders $m = 0, +2$ and squared fundamental spectra. The coincidence between these spectra means that SH spectra are $\sim\sqrt{2}$ times wider than the fundamental one in the frequency scale. While the SH spectrum width is independent of the fundamental spot size, the shape of the SH spectrum does depend on the fundamental spot size. The highest SH power of the central SH beam was up to 1 μW, resulting in 10^{-6} SHG efficiency. It is expected that SHG efficiency via NRND can be increased a few orders of magnitude using 2D nonlinear photonic structures, as predicted in [22].

Table 1. Comparison between Predicted and Measured NRND Order Parameters

NRND Order	Prediction [deg]	Measurement [deg]	
		Positive	Negative
0	0	0 ± 0.01	
1	2.29	2.30 ± 0.01	2.31 ± 0.01
2	4.59	4.66 ± 0.01	4.64 ± 0.01
3	6.89	6.93 ± 0.01	6.94 ± 0.01
4	9.21	9.13 ± 0.11	9.21 ± 0.01
5	11.54	11.67 ± 0.05	11.52 ± 0.01

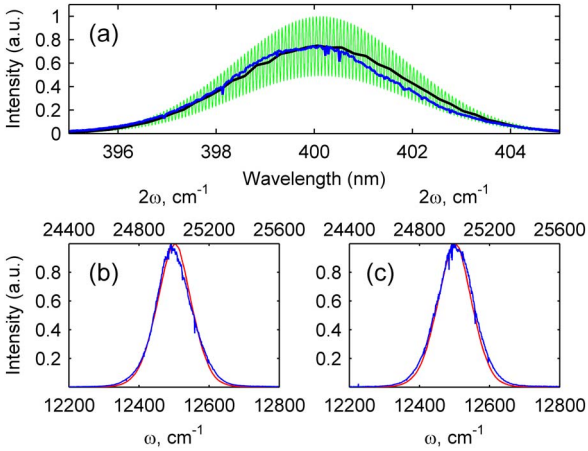

Fig. 4. (a) Calculated (green), averaged (black), and measured (blue) SH spectra for NRND order $m = +2$. Measured squared fundamental (red) and SH spectra (blue) for NRND order (b) $m = 0$ and for (c) $m = +2$.

In summary, we have studied nonlinear Raman–Nath diffraction of femtosecond laser pulses in a 1D periodic nonlinear photonic structure. The calculated second-harmonic spectra represent frequency combs for different orders of transverse phase matching. These frequency combs are in a close analogy with the well-known spectral Maker fringes observed in single crystals. We have found that the group-velocity mismatch between fundamental and second-harmonic pulses causes narrowing of the SH peaks. The spectral intensity of the second harmonic experiences a redshift with the propagation angle, which is opposite to the case of Čerenkov nonlinear diffraction. This spectral shift grows with the order of transverse phase matching. The calculated angular positions of individual SH beams and their angular and spectral widths are in good agreement with the experimental ones. A technique based on nonlinear Raman–Nath diffraction can be applied for nondestructive characterization of periodic domain structures in ferroelectric crystals.

This work was partially supported by the Grant of the President of the Russian Federation MK-250.2013.2, Krasnoyarsk Regional Fund for Science and Technical Activity Support and by the RAS grant no. 24.31. A. A. acknowledges the financial support of young scientists through the Ural Federal University Development Program. The authors thank A. S. Chirkin and I. V. Timofeev for fruitful discussions and A. V. Barannik for optical microscopy of the samples.

References

1. I. Freund, Phys. Rev. Lett. **21**, 1404 (1968).
2. S. M. Saltiel, D. N. Neshev, R. Fischer, W. Krolikowski, A. Arie, and Yu. S. Kivshar, Phys. Rev. Lett. **100**, 103902 (2008).
3. S. M. Saltiel, D. N. Neshev, W. Krolikowski, A. Arie, O. Bang, and Yu. S. Kivshar, Opt. Lett. **34**, 848 (2009).
4. K. Kalinowski, P. Roedig, Y. Sheng, M. Ayoub, J. Imbrock, C. Denz, and W. Krolikowski, Opt. Lett. **37**, 1832 (2012).
5. R. Fischer, S. M. Saltiel, D. N. Neshev, W. Krolikowski, and Yu. S. Kivshar, Appl. Phys. Lett. **89**, 191105 (2006).
6. A. S. Aleksandrovsky, A. M. Vyunishev, A. I. Zaitsev, A. V. Zamkov, and V. G. Arkhipkin, J. Opt. A **9**, S334 (2007).
7. I. V. Shutov, I. A. Ozheredov, A. V. Shumitski, and A. S. Chirkin, Opt. Spectrosc. **105**, 79 (2008).
8. K. A. Kuznetsov, G. Kh. Kitaeva, A. V. Shevlyuga, L. I. Ivleva, and T. R. Volk, JETP Lett. **87**, 98 (2008).
9. P. Molina, M. Ramírez, and L. Bausá, Adv. Funct. Mater. **18**, 709 (2008).
10. S. M. Saltiel, Y. Sheng, N. Voloch-Bloch, D. N. Neshev, W. Krolikowski, A. Arie, K. Koynov, and Y. S. Kivshar, IEEE J. Quantum Electron. **45**, 1465 (2009).
11. X. Deng, H. Ren, H. Lao, and X. Chen, J. Opt. Soc. Am. B **27**, 1475 (2010).
12. A. S. Aleksandrovsky, A. M. Vyunishev, A. I. Zaitsev, A. A. Ikonnikov, and G. I. Pospelov, Appl. Phys. Lett. **98**, 061104 (2011).
13. A. M. Vyunishev, A. S. Aleksandrovsky, A. I. Zaitsev, and V. V. Slabko, Appl. Phys. Lett. **101**, 211114 (2012).
14. A. M. Vyunishev, A. S. Aleksandrovsky, A. I. Zaitsev, and V. V. Slabko, J. Opt. Soc. Am. B **30**, 2014 (2013).
15. H. Ren, X. Deng, Y. Zheng, N. An, and X. Chen, Opt. Lett. **38**, 1993 (2013).
16. Y. Sheng, W. Wang, R. Shiloh, V. Roppo, A. Arie, and W. Krolikowski, Opt. Lett. **36**, 3266 (2011).
17. Y. Chen, W. Dang, Y. Zheng, X. Chen, and X. Deng, Opt. Lett. **38**, 2298 (2013).
18. Y. Sheng, Q. Kong, W. Wang, K. Kalinowski, and W. Krolikowski, J. Phys. B **45**, 055401 (2012).
19. V. Y. Shur, J. Mater. Sci. **41**, 199 (2006).
20. D. H. Jundt, Opt. Lett. **22**, 1553 (1997).
21. A. S. Aleksandrovsky, A. M. Vyunishev, A. I. Zaitsev, A. A. Ikonnikov, G. I. Pospelov, V. E. Rovskii, and V. V. Slabko, Quantum Electron. **41**, 748 (2011).
22. W. Wang, Y. Sheng, V. Roppo, Z. Chen, X. Niu, and W. Krolikowski, Opt. Express **21**, 18671 (2013).